Izvestiya, Physics of the Solid Earth, Vol. 39, No. 5, 2003, pp. 418–427. Translated from Fizika Zemli, No. 5, 2003, pp. 75–84.

Tidal Components in the Electrotelluric Field

A. N. Krolevets* and G. N. Kopylova**

**Kamchatka State Pedagogical University, Petropavlovsk-Kamchatski, Russia*

***Kamchatka Experimental Methodological Seismological Department, Geological Service, Russian Academy of Sciences, Petropavlovsk-Kamchatski, Russia*

Received July 18, 2002

Abstract—Long-term observations of the telluric potential difference on the measuring lines ($L \approx 100$ m) at the Verkhnyaya Paratunka (VP) and Tundrovyi sites on the Kamchatka Peninsula were used to study the tidal response of the electrotelluric field (ETF). This was accomplished by comparing the inferred amplitudes and phases of the harmonic ETF components M_2, O_1, S_1, etc., with the theoretical amplitudes and phases of the respective tidal waves [Melchior, 1968]. Quasi-stationary ETF components with frequencies of the tidal waves O_1, M_2, K_1, P_1, S_1, and S_2, recognizable at both sites, have amplitudes of a few units of μV/m. The VP time–distance curves of the vectors of the M_2 and O_1 ETF components have an elliptical shape, with their extreme points coinciding in time with phases of 0 and π rad of the tidal waves, implying that the M_2 and O_1 ETF components are directly related to the respective tides. This relationship is not observed in the ETF components with frequencies of the K_1, P_1, S_1, and S_2 waves, indicating that different factors were responsible for their formation, with tidal effects playing an insignificant role. The strain sensitivity of the ETF measuring system at the VP site was estimated; these estimates may prove useful in searching for ETF anomalies premonitory of strong earthquakes. A phenomenological model proposed in our work interprets the behavior of the M_2 and O_1 ETF components at the VP site in terms of percolation processes in a composite medium containing isotropic and anisotropic layers.

INTRODUCTION

By measuring the voltages between pairs of electrodes in the ground, it is possible to evaluate the gradient of the scalar potential of the Earth's electromagnetic (EM) field (electrotelluric field (ETF)). The ETF has been recorded for a few decades in various seismically active regions, including Kamchatka, with the aim of detecting earthquake precursors [Sobolev, 1993] under the assumption that the processes of earthquake preparation can have signatures in ETF variations via mechanoelectric conversion mechanisms. These mechanisms involve electrokinetic phenomena, the piezoelectric effect, and the electrification of the medium due to its fracture and friction [Sadovskii, 1982]. However, despite the often reported observations of various ETF variations in relation to earthquakes, no unambiguous idea of general patterns inherent in such variations exists. This is related to the difficulty in interpreting ETF time series due to the combined effect of diverse external and internal factors of ionospheric, meteorological, anthropogenic, and other origins that can produce specific ETF variations within a wide frequency range prior to any earthquake and impede the identification of signals related to seismicity.

One of the ways of estimating ETF sensitivity to variations in the stress–strain state of the medium is to examine the ETF response to tidal forces in the solid Earth. Tides can initiate mechanoelectric conversion mechanisms sensitive to small variations in strains and/or mechanical stresses in the frequency range of tidal forces. The deterministic nature of the tidal effect on the Earth [Melchior, 1968] allows one to study the ETF tidal response by comparing the phases and magnitudes of the experimentally inferred harmonic ETF components with the theoretical phases and amplitudes of the tidal potential, as well as with other tidal characteristics. The goal of this work is to investigate the tidal response of the ETF using observations in two Kamchatka areas as an example.

STUDY DATA

Since 1996, the Kamchatka Experimental Methodological Seismological Department, Geological Service, Russian Academy of Sciences, has monitored the ETF at the Verkhnyaya Paratunka (VP) and Tundrovyi (TN) sites (Fig. 1) using a geophysical radiotelemetering system at a 1-min sampling frequency [Moroz *et al.*, 1995; Balesta *et al.*, 1999]. The potential differences U on the VP and TN measuring lines (Figs. 1c, 1d) were recorded between two pairs of lead electrodes placed in holes at a depth of no less than 2 m in order to minimize temperature effects.[1] The lengths L and azimuths α of the measuring lines are presented in the table. The azimuths characterize the vectors directed from the

[1] The observation sites, lengths, and orientations of the measuring lines were chosen by Yu.F. Moroz, Institute of Volcanology, Geology, and Geophysics, Far East Division of the Russian Academy of Sciences.

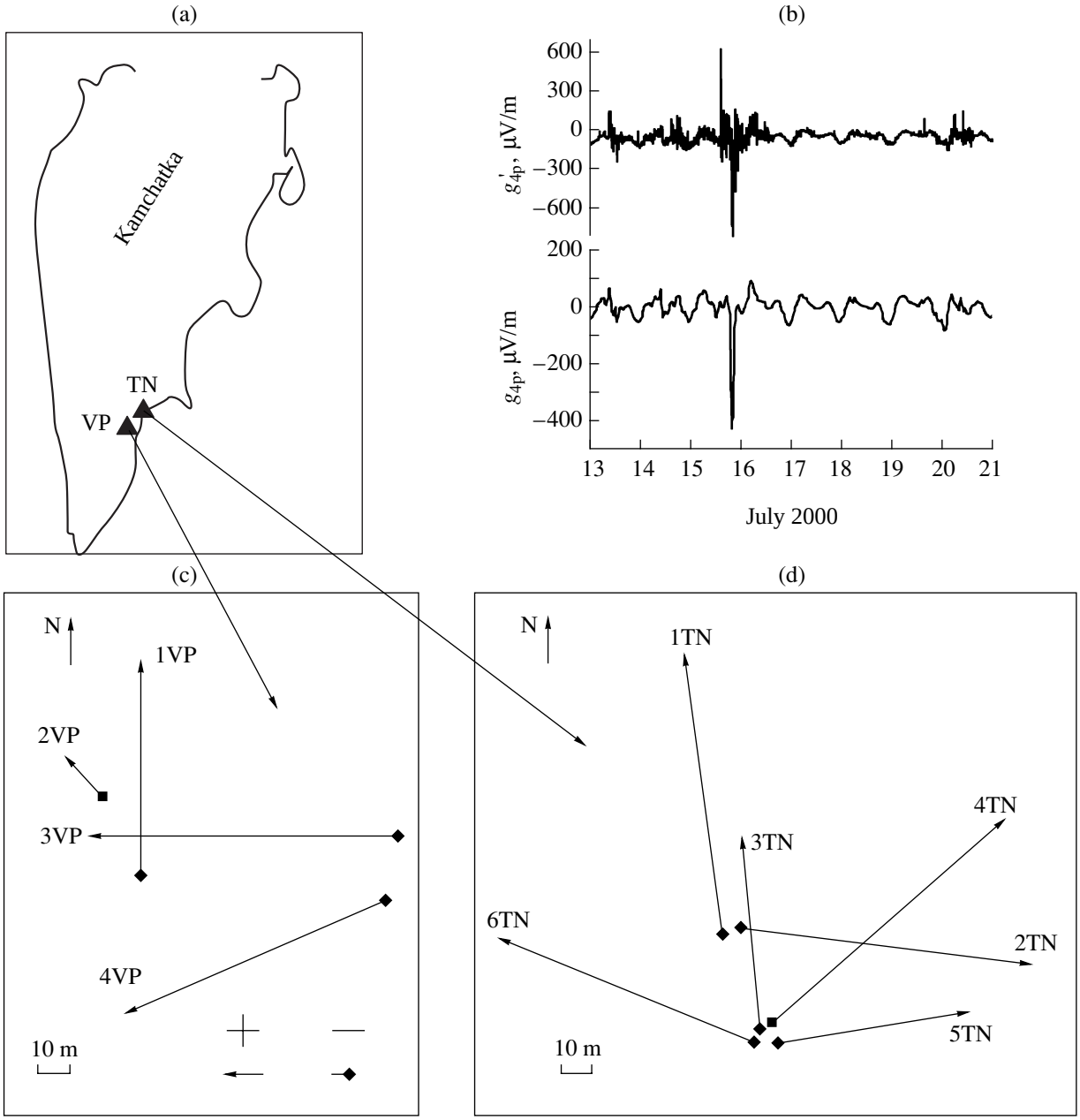

Fig. 1. Location of electrotelluric observation sites (a) and measuring lines at the VP (c) and TN (d) sites; (b) an example of a one-week observation of the electrotelluric potential difference on VP line 1: the lower and upper plots represent minute-by-minute observations and hourly averages, respectively.

conditionally negative electrodes to the conditionally positive ones. The U measurement uncertainty is 0.5 mV. We used a U time series four years and eight months long recorded at the VP station (from October 1, 1996) and a series one year long recorded at the TN station (from July 13, 2000). The overall length of measurement gaps is less than 1%.

The ETF measurements at both sites revealed diurnal and semidiurnal variations (Fig. 1b) ranging in amplitude from a few tens to a few hundreds of μV/m units, depending on the extent of geomagnetic disturbance and meteorological factors [Kopylova *et al.*, 2001]. Annual ETF periodicities and baylike ETF variations lasting from one day to a few tens of days are recognizable on all measuring lines. Such variations are primarily due to seasonal variations in the spontaneous polarization of the electrodes and to groundwater flows due to heavy rains or snow melt.

The measured data were preprocessed by calculating the parameter $g'_i = U_i/L_i$ for each ith line; this parameter is equal, within an accuracy of the noise component, to the projection of the scalar potential gra-

Characteristics of the VP and TN measuring lines and phases Δφ and amplitudes *s* of the O_1 and M_2 tidal components in the time series g_i

Site	Coordinates		Characteristics of lines			O_1 wave		M_2 wave	
	λ_0, deg (E)	ϕ_0, deg (N)	line *i*	length, m	azimuth, α, deg	Δφ, rad	*s*, μV/m	Δφ, rad	*s*, μV/m
Verkhnyaya Paratunka	158.12	52.83	1VP	70	0	2.53 ± 0.12	2.18 ± 0.18	–0.34 ± 0.14	1.62 ± 0.09
			2VP	20	320	–	–	–	–
			3VP	100	270	0.03 ± 0.10	1.63 ± 0.05	–2.84 ± 0.05	1.73 ± 0.05
			4VP	100	225	0.37 ± 0.02	2.32 ± 0.15	–3.07 ± 0.02	1.99 ± 0.07
Tundrovyi	158.79	53.07	1TN	97	350	2.45 ± 0.06	3.66 ± 0.12	–	–
			2TN	105.5	94	0.68 ± 0.09	2.06 ± 0.07	–	–
			3TN	69	347	2.33 ± 0.03	3.11 ± 0.29	–	–
			4TN	102	49	–	–	–	–
			5TN	65	82	0.80 ± 0.07	2.34 ± 0.11	–	–
			6TN	90	302	2.28 ± 0.01	2.10 ± 0.14	–	–

dient of the Earth's EM field $\nabla\psi$ onto the direction of the corresponding line.[2] Then, in order to remove the low-frequency trend, the differences $g_i = \langle g_i' \rangle_1 - \langle g_i' \rangle_{48}$ were calculated at 1-h intervals, where $\langle g_i' \rangle_1$ are hourly averages and $\langle g_i' \rangle_{48}$ are 48-h moving window averages. The resulting g_i time series were then analyzed.

The ETF at the TN site is affected by an anthropogenic factor due to the proximity of the settlement (a few hundred meters from the measuring lines). The anthropogenic effect is responsible for characteristic daily and weakly periodicities in the variance of the *U* time series. The variances of the g_i time series estimated from 24-h series of observations on the TN lines, are 1.3 to 1.4 times higher than those on the VP lines. In some time intervals, the variance range of the TN g_i series is a few tens of times wider compared to the VP lines. This effect of higher noise in the *U* and g_i series at the TN site is due to the permanently present anthropogenic effect of the settlement and to the periodic operation of powerful EM facilities.

IDENTIFICATION OF TIDAL ETF COMPONENTS

Quasi-stationary tidal components. Procedures of synchronous stacking of signals were applied to the $g_i(t)$ series within the range of periods T = 11–27 h at a step of $1/T$ [Serebrennikov and Pervozvanskii, 1965], after which the amplitudes s_i and phases of the principal harmonics of the stacked signal were determined. The procedure of synchronous stacking was previously applied to the tidal response in high-frequency seismic noise (HFSN) [Saltykov *et al.*, 1997]. The full algorithm for identifying the phase and amplitude of the tidal signal in impulsive EM radiation (IEMR) was used by Krolevets and Pavlyukov [2000].

The periodogram of the g_{4p} series (Fig. 2) reveals the expected peaks of the signals at frequencies corresponding to the tidal waves M_2, O_1, P_1, K_1, S_1, and S_2 [Melchior, 1968]. Peaks at periods of the tidal waves S_1 (24.00 h), S_2 (12.00 h), and O_1 (25.82 h) are reliably identifiable above the noise level in the $g_i(t)$ periodograms on VP lines 1, 3, and 4 and on TN lines 1–3, 5, and 6. Peaks of M_2 (12.42 h), K_1 (23.93 h), and P_1 (24.07 h) are observed in the $g_i(t)$ periodograms on VP lines 1, 3, and 4.

The periodicities coinciding in frequency with the waves S_1, S_2, K_1, and P_1 cannot be directly related to the tidal effect. The S_1 and S_2 periodicities can be due to the solar diurnal variations in the geomagnetic field of the S_q type [Yanovskii, 1964] and to other factors. The periodicities at frequencies of the K_1 and P_1 waves can be composite signals of the diurnal and annual frequencies. In any case, it appears impossible to separate the actual tidal response of the K_1 and P_1 waves from the signal caused by the aforementioned factors. However, reliable identifications of the O_1 and M_2 signals in the g_i variations on three of the four VP lines and the O_1 signals on the majority of the TN lines are evidence of nearly stationary tidal components present in the ETF variations.

No signatures of O_1 and M_2 waves are recognizable in the VP variations $g_2(t)$ (table). Line 2p is not longer than 20 m, and its length is insufficient for extracting tidal ETF signals from noise even after their stacking over more than four years. Signals at the M_2 frequency were not identified on TN lines (table) apparently due to the high level of anthropogenic noise.

[2] We do not relate g_i' directly to the corresponding projections of the electric field because g_i' includes uncontrollable noise, and the intensity of the electric field **E** includes not only the scalar potential gradient $-\nabla$, but also the induction term $-\partial\mathbf{A}/\partial t$, where **A** is the vector potential of the EM field.

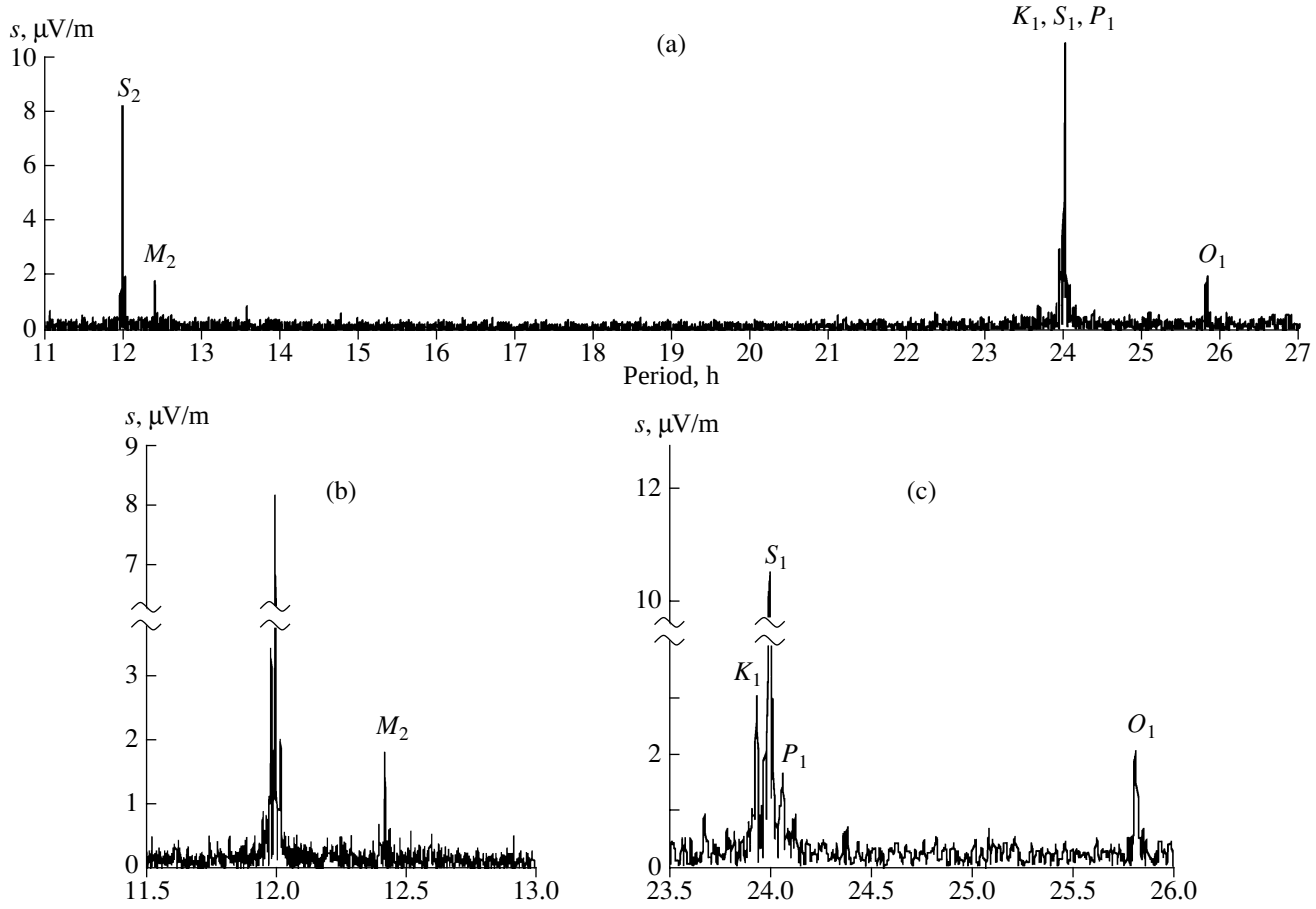

Fig. 2. Periodogram of telluric potential variations on VP line 4 in period ranges of (a) 11–27 h, (b) 11.5–13 h, and (c) 23.5–26 h.

Temporal variations in the tidal response. The procedures of synchronous stacking of signals having periods of tidal waves were applied with a step of 3 h to g_i series in moving windows of 672 h (O_1 wave) and 696 h (M_2 wave). The window lengths were chosen so as to prevent the intense 12- and 24-h harmonics from penetrating into the windows [Marple, 1990]. We then determined the amplitudes $s_{ij}(t)$ and phases $\varphi_{ij}(t)$ of the principal harmonics of the stacked signal on each line (denoted by the subscript i) for each of the O_1 and M_2 waves (the subscript j). The amplitude $s_{ij}(t)$ in a current window is a window average, and the phase $\varphi_{ij}(t)$ was taken at the midwindow point. The phases of the tidal potential $\Phi_j(t)$ calculated at the same time moments were then subtracted from the $\varphi_{ij}(t)$ values [Melchior, 1968; Bagmet *et al.*, 1989]. The phase differences $\Delta\varphi_{ij}(t) = \varphi_{ij}(t) - \Phi_j(t)$ were calculated modulo 2π.

The temporal variations of the phase difference $\Delta\varphi_{4p,\,O1}(t)$ and amplitude $s_{4p,\,O1}(t)$ are plotted in Fig. 3. The amplitude of the signal $s_{4p,\,O1}(t)$ (Fig. 3b) varies from 0 to 8 μV/m, averaging about 2 μV/m, which agrees with the value $s_{4p,O1} \approx 2$ μV/m determined from the periodogram (Fig. 2c).

The variations in $\Delta\varphi_{4p,\,O1}(t)$ (Fig. 3a) have periods of relatively stable behavior when the $\Delta\varphi$ values are close to their average and their variance is close to zero, as well as periods during which the scatter in the $\Delta\varphi$ values is close to the maximum possible value 2π. In the latter case, the phase difference is indefinite. As a rule, the time intervals of minimum amplitudes s coincide with those of indefinite $\Delta\varphi$ values. The tidal signal/noise ratio in these intervals of the g_i series decreases to such an extent that the tidal signal is undetectable. The noise level is so high that the $s_{ij}(t)$ values cannot be unambiguously interpreted as the tidal response amplitudes because, in some time intervals, the noise components at frequencies of the O_1 and M_2 waves are comparable in amplitude with the tidal response or even exceed it.

Krolevets and Pavlyukov [1999] showed that a criterion for the existence of a stationary signal in a series with a high noise level is the tendency of the inferred phase differences $\Delta\varphi_{ij}(t)$ to take on a definite (true!) value. Based on the ETF observations on VP lines 1, 3, and 4, such $\Delta\varphi_{ij}(t)$ values for the O_1 and M_2 waves are identifiable from histograms (Fig. 4). Distinct maximums in the histograms at well-defined values indicate the existence of nearly stationary components at the

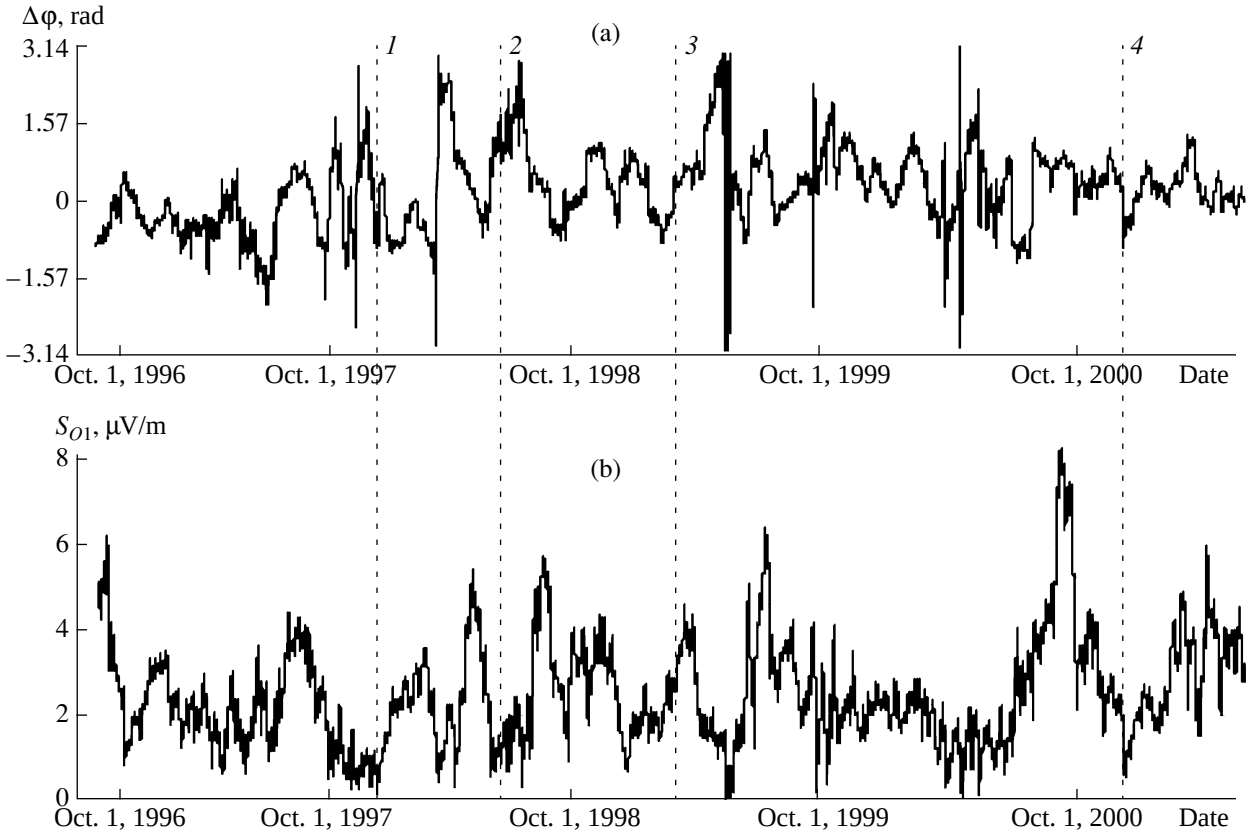

Fig. 3. Temporal variations in (a) the phase difference Δφ and (b) the amplitude *s* of the O_1 ETF component on VP line 4. Vertical lines mark the earthquakes: (*1*) December 5, 1997, $M = 7.9$; (*2*) June 1, 1998, $M = 6.3$; (*3*) March 8, 1999, $M = 6.9$; (*4*) December 20, 2000, $M = 5.6$.

frequencies of the O_1 and M_2 waves. The table presents the average phase shifts $\Delta\varphi_{ij}(t)$ and amplitudes $s_{ij}(t)$ of the projections $g_{ij} = (\nabla\psi)_{ij}$ of the ETF tidal components O_1 and M_2 along the measuring line directions.

Reconstructing the structure of the ETF tidal components. The out-of-phase nature of the components at frequencies of the O_1 and M_2 waves in the VP signals (Fig. 4) and at a frequency of the O_1 wave in the TN signal (table) is evidence of a nonlinear polarization of $\mathbf{g}_j$ in the medium. Assuming that the instantaneous vector values of the stationary tidal component of a *j*th wave $\mathbf{g}_j = \nabla\psi_j$ depend solely on the wave phase (i.e., $\mathbf{g}_j = \mathbf{g}_j(\Phi_i)$), one can estimate the vector projections of the *j*th tidal wave component $g_{x,j}$ and $g_{y,j}$ on the *Ox* (eastward) and *Oy* (northward) axes. The number of the VP and TN lines is sufficient to perform this procedure by the least-squares method with additional noise filtering.

A function of residuals was calculated for each wave type:

$$R_j = \sum_i (g_{i,j} - (g_{x,j}\sin\alpha_i + g_{y,j}\cos\alpha_i))^2,$$

where *i* is the index of summation over all lines of a given site. The unknown projections $g_{x,j}$ and $g_{y,j}$ onto the coordinate axes are determined by solving the system of equations

$$\partial R_j/\partial g_{x,j} = 0, \quad \partial R_j/\partial g_{y,j} = 0.$$

For the VP site, the final expressions take the form

$$\begin{aligned} g_{x,j}(\Phi_j) &= -\frac{1}{4}(\langle g_{p1}\rangle + 3\langle g_{p3}\rangle + \sqrt{2}\langle g_{p4}\rangle), \\ g_{y,j}(\Phi_j) &= -\frac{1}{4}(3\langle g_{p1}\rangle + \langle g_{p3}\rangle - \sqrt{2}\langle g_{p4}\rangle), \end{aligned} \quad (1)$$

where the broken brackets denote averaging over all time moments with identical phase values of the tidal waves under study. Since the sampling intervals of the $g_i(t)$ series (1 h) and the periods of the O_1 and M_2 waves are incommensurate, we averaged not the exact g_i values at required time moments but the nearest hourly averages. The expressions for the TN site similar to (1) are more cumbersome due to the greater number of lines and fractional values of their azimuths.

The points in Fig. 5 are the ends of the O_1 (Fig. 5a) and M_2 (Fig. 5b) wave vectors $\mathbf{g}_j(\Phi_j) = (g_{x,j}, g_{y,j})$ in the VP area obtained from (1). The phase values Φ_j are given near these points. Arrows show the rotation sense of the time–distance curve (clockwise for O_1 and counterclockwise for M_2). Each plot presents $\mathbf{g}_j(\Phi_j)$ values

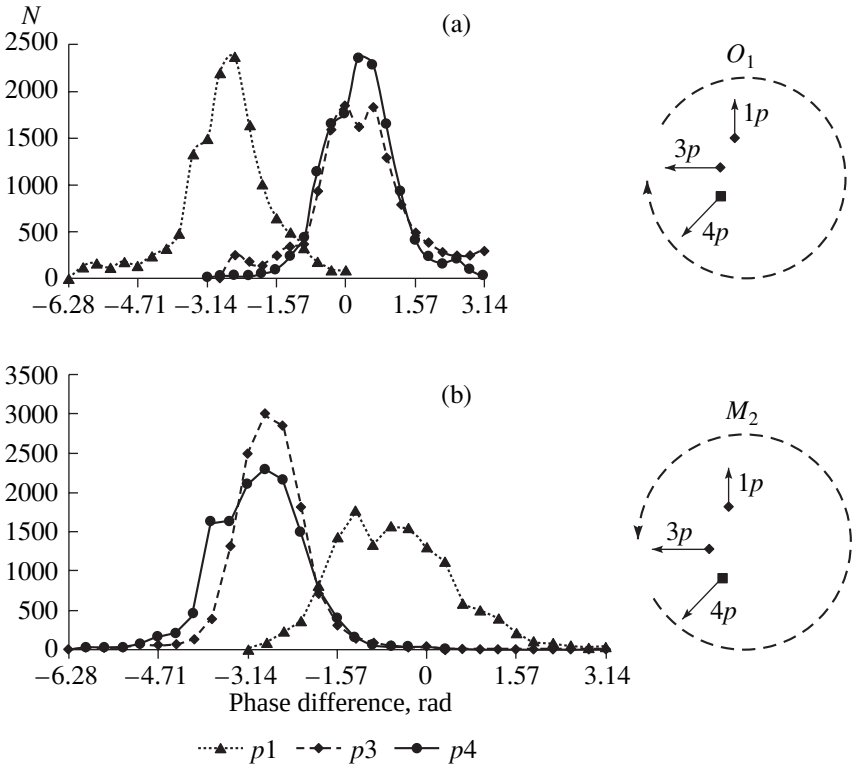

Fig. 4. Histograms of the phase differences $\Delta\varphi_{ij}$ of the harmonic components (a) O_1 and (b) M_2 in the ETF projections on VP lines 1, 3, and 4. Arrows on the right indicate the alternations of the phases on the measuring lines.

obtained from the first and second halves of each g_i observation series. This representation allows estimation of the uncertainty and stability of $\mathbf{g}_j(\Phi_j)$ calculations.

The phase differences at adjacent points, with the exception of the end points of the synchronous stacking time window, differ by a value obtained from the 1-h sampling interval conversion into a phase. The phase differences at the end points differ by a value obtained by the phase conversion of the fractional part ΔT of the wave period expressed in hours (25.82 – 25.0 = 0.82 h for O_1 and 12.42 – 12.0 = 0.42 h for M_2). This feature of the algorithm in question increases, to an extent, the determination uncertainties at the end points of the $\mathbf{g}_j(\Phi_j)$ time–distance curve compared to the other points.

Similar plots obtained from the TN data are not given because the behavior of the calculated values $\mathbf{g}_j(\Phi_j) = (g_{x,j}, g_{y,j})$ is unstable due to the strong distortion of the ETF tidal components by noise.

DISCUSSION

The possibility of identifying the O_1 and M_2 ETF components arises from the fact that the tidal forces at these frequencies are rather intense and the related ETF signals are less noisy compared to K_1, P_1, and S_2.

The structure and mechanism of the ETF tidal response in the VP area. The time–distance curves of the vectors $\mathbf{g}_j(\Phi_j) = (g_{x,j}, g_{y,j})$ for the O_1 and M_2 waves (Figs. 5a, 5b) obtained by averaging over nonoverlapping intervals longer than two years are fairly stable, enabling both qualitative and quantitative estimation of the ETF tidal response. The time–distance curves of the vectors $\mathbf{g}_{O1}$ and $\mathbf{g}_{M2}$ are nearly elliptical in shape. The major axes of the ellipses pass through the points of the $\mathbf{g}_j$ curves coinciding in time with moments when the O_1 and M_2 harmonic components of the tidal potential assume extreme values and their phases are $\Phi_j = 0$ and $\Phi_j = \pi$. The major axes of the ellipses in Figs. 5a and 5b are indicated by vectors directed toward the value $\Phi_j = 0$. The azimuth of the O_1 axis is nearly 210° SW. The M_2 azimuth is nearly 60° NE. Note that the inversion of the $\mathbf{g}_j$ rotation sense for the O_1 (clockwise) and M_2 (counterclockwise) waves is accompanied by the direction inversion of the major axis of the ellipse.

The coincidence in time of the time–distance extreme points of the g_{O1} and g_{M2} vectors with the extreme values of the respective *earth tide* potentials indicates a direct relationship between the corresponding ETF and earth tide components. Thus, the ETF components in the VP area with frequencies of the O_1 and M_2 waves are directly related to the *tidal* force acting on the solid Earth.

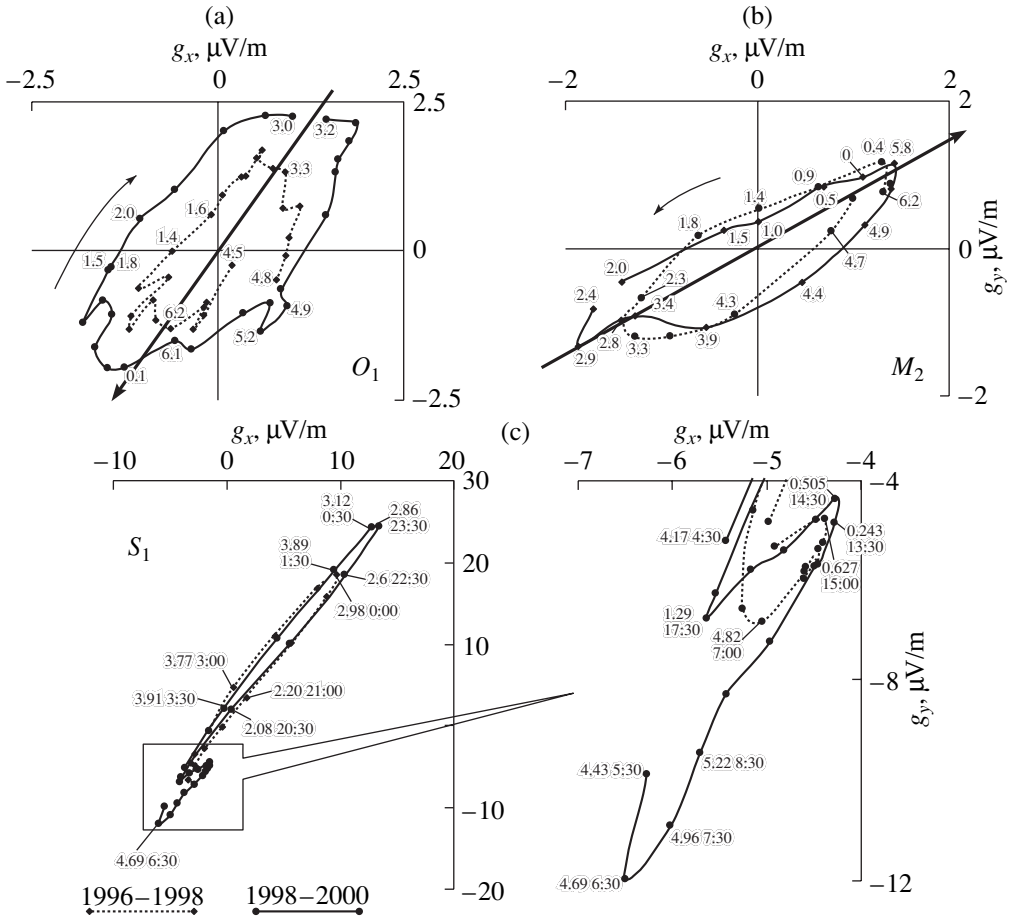

Fig. 5. Characteristics of the ETF components (a) O_1, (b) M_2, and (c) S_1 in the VP area.

The effect of oceanic tides on the ETF variations in coastal areas of eastern Kamchatka was examined by Sobolev and Morozov [1974], who showed that variations in the height of the oceanic tide coincide in frequency with variations in the earth tide, but their phases significantly differ. If the phase of the ocean tide wave is set at zero at the time of the highest sea level, the phase of the O_1 ocean tide in the Petropavlovsk-Kamchatski area is 0.90 rad ahead of the O_1 earth tide phase, and the phase of the M_2 ocean tide is 2.46 rad behind the phase of the M_2 earth tide phase.[3] The extreme values of the ocean tide have no signatures in the $\mathbf{g}_j$ time–distance curves, indicating that the ocean tide has no significant effect on the O_1 and M_2 ETF components in the VP area.

The electric currents in the oceanic regions surrounding Kamchatka and particularly in the Kuril–Kamchatka deep-sea trench area can substantially affect the EM field on land due to the coast effect [Moroz, 1991; Rokityanskii, 1963]. Characteristic variations in the EM field structure are observable at distances ranging from a few kilometers to tens of kilometers from the coastline and depend on its characteristics and the seafloor topography.

Sobolev and Morozov [1974] characterized ETF variations of the S_q type in eastern Kamchatka areas and showed that their time–distance curves at various stations are nearly elliptical, with the major axis oriented parallel to the maximum gradient of the seafloor depth. The VP site is located at a distance of about 20 km from the coastline. An SW–NE elongation of the O_1, M_2, and S_1 ETF polarization ellipses (Fig. 5) suggests that the coast effect influences the ETF formation. On the other hand, the opposite directions of the motion of the $\mathbf{g}_{O1}$ and $\mathbf{g}_{M2}$ vectors cannot be accounted for by the coast effect.

Several mechanisms responsible for the ETF effect of the tidal force are conceivable. These mechanisms can operate both separately and jointly. First, the tidal volume deformation of a fluid-saturated medium can cause groundwater motion coinciding in phase with the variation in its pore pressure. The resulting electrokinetic phenomena lead to the generation of periodical

[3] Our calculations are based on measurements of the ocean tide height in the Avachinskaya Bay during the year 2000. The measurements were performed by the Kamchatka Territorial Department of Hydrometeorology and Environmental Monitoring.

ETF components. This mechanism is most likely. Second, one cannot rule out the piezoelectric effect in quartz-bearing rocks of the area. Third, the tidal effect acting on the ionosphere, the magnetosphere, and the Earth's liquid core and thereby on their electric currents, as well as on ferromagnetic rocks of the crust and mantle, can generate the inductive component of the electric field near the Earth's surface, and this component is transformed into the ETF due to electrical conductivity inhomogeneities in the near-surface layer.

The time–distance patterns of the O_1 and M_2 waves suggest the simultaneous involvement of at least two mechanisms producing the ETF tidal components. The first mechanism may be directly related to tidal forces. The W_{O1} and W_{M2} components of the tidal potential are the westward traveling spherical harmonics

$$W_{O1} = C_{O1}\sin(2\phi)\cos(\omega_{O1}t + (\lambda - \lambda_0)),$$

$$W_{M2} = C_{M2}\cos^2(\phi)\cos(\omega_{M2}t' + 2(\lambda - \lambda_0)),$$

where λ and ϕ are the coordinates of an arbitrary point on the Earth's surface; λ_0 and ϕ_0 are the coordinates of the observation sites (table); ω_j are the frequencies $\omega_{O1}t + (\lambda - \lambda_0) = \Phi_{O1}$ and $\omega_{M2}t' + 2(\lambda - \lambda_0) = \Phi_{M2}$; C_j are the amplitudes of the spherical harmonics; and t and t' are the times measured for each wave type from the moment when the respective tidal potentials assume their maximum values at the observation point.

Let $\mathbf{f}_j = \nabla W_j$ denote the gradient of the tidal potential equal in absolute value to the specific tidal force but opposite to it in direction. Then, the projections of the tidal potential gradient are

$$f_{y,O1} = 2C_{O1}\cos(2\phi)\cos(\Phi_{O1})/a,$$
$$f_{x,O1} = 2C_{O1}\sin(\phi)\sin(\Phi_{O1})/a, \quad (2)$$

$$f_{y,M2} = -C_{M2}\sin(2\phi)\cos(\Phi_{M2})/a,$$
$$f_{x,M2} = 2C_{M2}\cos(\phi)\sin(\Phi_{M2})/a, \quad (3)$$

where a is the Earth's mean radius.

Relations (2) and (3) describe, in the parametric form, the equations of ellipses whose axes are directed exactly toward the cardinal points. As the Φ_j parameter varies from 0 to 2π, the time–distance curves of the $\mathbf{f}_{O1}$ and $\mathbf{f}_{M2}$ vectors rotate along the ellipse clockwise. At $\Phi_j = 0$ and $\Phi_j = \pi$, the vectors $\mathbf{f}_j$ at the latitude of the observations ($\phi = \phi_0 = 52.8°$ N) are directed southward and northward, respectively. One can assume that one of the generation mechanisms for the ETF tidal component gives rise to the regular ETF component $\mathbf{g}_j^p$ that is similar to the tidal force:

$$\mathbf{g}_j^p = \delta_j \mathbf{f}_j,$$

where δ_j is the coefficient of proportionality. Such a mechanism can be implemented through mechanoelectric converters related to the groundwater percolation in an isotropic medium.

Another mechanism assumes a correlated behavior of the horizontal ETF components and the tidal potential and, accordingly, tidal volume strains [Melchior, 1968]:

$$\mathbf{g}_{j,y}^c = -\beta_j\cos(\Phi_j), \quad g_{j,y}^c = -\gamma_j\cos(\Phi_j),$$

where β_j and Φ_j are coefficients of proportionality.

This mechanism can be supported by both inductive processes in the medium of the study area [Berdichevsky and Zhdanov, 1985] and percolation processes in a strongly anisotropic medium due to tidal volume expansion (contraction). Media isotropic and anisotropic in percolation properties can be separated spatially, for example, in depth. This assumption is supported by data on the geological and hydrogeological conditions in the study area. The upper part of the geological section here includes two rock sequences differing in their percolation properties: the upper sequence of loose Quaternary sediments with groundwater moving predominantly through pores (an isotropic medium) and the lower sequence of volcanic–sedimentary rocks dominated by fracture-type groundwater circulation (an anisotropic medium) [Manukhin and Vorozheikina, 1976].

The time–distance curves of the total vectors of the ETF tidal components $\mathbf{g}_j = \mathbf{g}_j^c + \mathbf{g}_j^r$ are elliptical in shape and rotate either clockwise if δ, β, and γ are positive or counterclockwise if δ is positive and β and γ assume negative values and are sufficiently large in absolute value. The orientation and length of the time–distance ellipse axes and the direction of their rotation depend, first, on the relative values of δ, β, and γ and, second, on the type of tidal wave and the latitude. The β and γ values may also depend on the conductivity gradient in the medium. The rotation direction inversion of the $\mathbf{g}_j$ values calculated for the O_1 and M_2 waves is accompanied by a change in the directions of the major axes of the ellipses (Figs. 5a, 5b). Extreme points of the time–distance curves correspond to the tidal potential phases 0 and π, as seen from real ETF time–distance curves (Figs. 5a, 5b). The model proposed above is phenomenological, and its physical interpretation requires further examination.

The structural patterns of the S_1 ETF component. The S_1 wave period is exactly 24 h, making it possible to determine not only the tidal wave phases but also the time of day (UT) from the $\mathbf{g}_{S1}$ time–distance plot (Fig. 5c). The latter can be divided into two parts according to its variation pattern. The right-hand part commences at 17:30 (or 5:30 local winter time, hereafter LT) and ends at ≈5:00 (17:00 LT). The horizontal ETF components in this part of the time–distance curve are highly correlated, and the absolute $\mathbf{g}_{S1}$ values are about an order of magnitude greater than the $\mathbf{g}_j$ values for O_1 and M_2. This "daytime" part of the time–distance curve reaches its extreme value at nearly exactly 0:00 (12:00 LT). The second part of the $\mathbf{g}_{S1}$ time–distance curve is nearly elliptical and spans night hours.

Extreme points of both parts of the curve are not matched by extreme values of the tidal potential, indicating that the S_1 ETF component cannot be due to tides.

The complicated pattern of the $\mathbf{g}_{S1}$ component indicates its complex origin. The effect of earth tides is far from being the primary factor responsible for this component. Actually, the amplitude of the S_1 wave of the earth tide potential is not the highest [Melchior, 1968] but the corresponding ETF amplitude is highest among ETF components (Figs. 2 and 5).

Estimation of the strain sensitivity of the ETF observation system in the VP area. The table gives the O_1 and M_2 tidal wave amplitudes measured on individual lines. The amplitudes range from 1 to 3.5 μV/m. Estimates of the $\mathbf{g}_{O1}$ and $\mathbf{g}_{M2}$ vectors in the VP area (Figs. 5a, 5b) also show that the ETF amplitudes of earth tide variations do not exceed a few units of μV/m. Theoretical values of the volume strain produced by the O_1 and M_2 tide components are on the order of 6×10^{-9} at the VP latitude [Bagmet *et al.*, 1989]. The strain sensitivity coefficient of the ETF measuring system in the VP area is estimated at about $(3–4) \times 10^3$ V/m. If volume strains on the order of 10^{-6} to -10^{-5} similar in period to the earth tide waves arise at preseismic stages of a strong earthquake in the VP area, such strains can be accompanied by ETF variations with amplitudes of a few to tens of μV/m units. This estimate is valid if the ETF response to variations in volume deformations is linear within a wide strain range exceeding the tidal range by three orders of magnitude or more.

Tidal response of the ETF in the VP area and seismicity. The vertical lines in Fig. 3 show the time moments of the strongest earthquakes of 1997–2000: (*1*) December 5, 1997, $M = 7.9$, $R = 354$ km; (*2*) June 1, 1998, $M = 6.3$, $R = 151$ km; (*3*) March 8, 1999, $M = 6.9$, $R = 148$ km; (*4*) December 20, 2000, $M = 5.6$, $R = 137$ km. These earthquakes were accompanied in the VP area by ground motion intensities of 3–4 to 5 on the MSK-64 scale. No regular variations in the amplitude $s_{i,O1}(t)$ and in the phase difference $\Delta\varphi_{i,O1}(t)$ were observed before these events. This behavior of the ETF O_1 signal differs for that of the O_1 signals in HFSN and IEMR. Preseismic processes of strong earthquakes enhance the regular pattern in the HFSN O_1 tidal component, giving rise to long-term stabilization of the phase difference $\Delta\varphi_{O1}$ [Saltykov *et al.*, 1997]. The O_1 and M_2 IEMR components distinct from noise appear exclusively at preseismic stages [Krolevets and Pavlyukov, 2000].

Applying multivariate statistical analysis to the ETF variations in the VP area, Kopylova *et al.* [2001], revealed a weak anomaly prior to the Kronotski earthquake of December 5, 1997 (earthquake *1* in Fig. 3). Supposedly, this anomaly was due to an increase in the level of noise components of signals recorded on the measuring lines. The unstable behavior of the phase difference of the ETF O_1 tidal component preceding the Kronotski earthquake (Fig. 3) likewise indicates an increase in the level of noise components in the ETF time series preceding this earthquake.

However, comparison of $s_{ij}(t)$ and $\Delta\varphi_{ij}(t)$ with the times of strong earthquakes does not allow one to decisively state that variations in the O_1 and M_2 tidal ETF signals are related to preseismic processes and earthquake occurrence. This problem requires further research.

CONCLUSIONS

(1) The electrotelluric field (ETF) in the vicinity of the Verkhnyaya Paratunka (VP) and Tundrovyi observation sites contains quasi-stationary components at frequencies of the O_1, M_2, K_1, P_1, S_1, and S_2 tidal waves.

(2) The VP patterns of the O_1 and M_2 ETF components are mainly due to the direct tidal effect on the solid Earth. During the periods of these tidal waves, the vectors of the corresponding ETF components describe time–distance curves of a nearly elliptical shape, rotating clockwise (O_1 wave) or counterclockwise (M_2 wave).

(3) The amplitudes of the ETF response to the tidal effects of the O_1 and M_2 waves amount to a few units of μV/m.

(4) A phenomenological model proposed in this paper interprets the behavior of the O_1 and M_2 ETF components in terms of the percolation processes in a composite medium containing isotropic and anisotropic layers.

REFERENCES

Bagmet, A.L., Bagmet, M.I., Barabanov, V.L., *et al.*, Study of Earth Tide Variations in the Groundwater Level in the Obninsk Hole, *Izv. Akad. Nauk SSSR, Fiz. Zemli*, 1989, no. 11, pp. 84–95.

Balesta, S.T., Kopylova, G.N., Latypov, E.R., and Kuz'min, Yu.D., Multidisciplinary Geophysical Observations in the Petropavlovsk, Kamchatka Research Site, *Vulkanol. Seismol.*, 1999, nos. 4–5, pp. 90–100.

Berdichevsky, M.N. and Zhdanov, M.S., *Interpretatsiya anomalii peremennogo elektromagnitnogo polya Zemli* (Interpretation of Anomalies in the Earth's Electromagnetic Field), Moscow: Nedra, 1981.

Kopylova, G.N., Lyubushin, A.A., Jr., and Taranova, L.N., Application of the Multivariate Statistical Analysis to the Data Processing of Electrotelluric Observations in Kamchatka, *Problemy geodinamiki i prognoza zemletryasenii* (Problems of Geodynamics and Earthquake Prediction), F.G., Korchagin, Ed., Khabarovsk: ITiG DVO RAN, pp. 225–245.

Krolevets, A.N. and Pavlyukov, V.K., *Initsiirovanie prilivnogo otklika impul'snogo elektromagnitnogo izlucheniya iz litosfery protsessami v ochagakh zemletryasenii* (Initiation of the Tidal Response of the Impulsive Electromagnetic Radiation from the Lithosphere by Processes in Earthquake Sources), Petropavlovsk-Kamchatski: KGPU, 1999.

Krolevets, A.N. and Pavlyukov, V.K., Tidal Response of the Impulsive Electromagnetic Radiation and Short-Term Pre-

diction of Strong Earthquakes, *Problemy seismichnosti Dal'nego Vostoka* (Far East Seismicity Problems), Petropavlovsk-Kamchatski: KOMSP GS RAN, 2000, pp. 175–185.

Manukhin, Yu.F. and Vorozheikina, L.A., Hydrogeology of the Paratunka Hydrothermal System and the Conditions of Its Formation, *Gidrotermal'nye sistemy i termal'nye polya Kamchatki* (Hydrothermal Systems and Thermal Fields in Kamchatka), V. Sugrobov, Ed., Vladivostok: DVNTs AN SSSR, 1976, pp. 143–178.

Marple, S.P., Jr., *Tsifrovoi spektral'nyi analiz i ego prilozheniya* (Digital Spectral Analysis and Its Applications), Moscow: Mir, 1990.

Melchior, P., *The Earth Tides*, Oxford, 1966. Translated under the title *Zemnye prilivy*, Moscow: Mir, 1968.

Moroz, Yu.F., *Elektroprovodnost' zemnoi kory i verkhnei mantii Kamchatki* (Electrical Conductivity of the Crust and Upper Mantle of Kamchatka), Moscow: Nauka, 1991.

Moroz, Yu.F., Bakhtiarov, V.F., Voropaev, V.F., *et al.*, Electrotelluric Field Monitoring in Relation to the Prediction of Strong Earthquakes in Kamchatka, *Vulkanol. Seismol.*, 1995, nos. 4–5, pp. 139–149.

Rokityanskii, I.I., Coastal Effect in Earth's Electromagnetic Field Variations, *Izv. Akad. Nauk SSSR, Ser. Geofiz.*, 1963, no. 12, pp. 1814–1822.

Sadovskii, M.A., Ed., *Elektromagnitnye predvestniki zemletryasenii* (Electromagnetic Precursors of Earthquakes), Moscow: Nauka, 1982.

Saltykov, V.A., Sinitsyn, V.I., and Chebrov, V.N., Stress-Induced Variations in the Tidal Component of the High-Frequency Seismic Noise, *Vulkanol. Seismol.*, 1997, no. 4, pp. 73–83.

Serebrennikov, M.G. and Pervozvanskii, A.A., *Vyyavlenie skrytykh periodichnostei* (Identification of Hidden Periodicities), Moscow: Nauka, 1965.

Sobolev, G.A., *Osnovy prognoza zemletryasenii* (Fundamentals of Earthquake Prediction), Moscow: Nauka, 1993.

Sobolev, G.A. and Morozov, V.N., Identification of Earthquake Precursors in the Electrotelluric Field *Seismichnost' i seismicheskii prognoz, svoistva verkhnei mantii i ikh svyaz' s vulkanizmom na Kamchatke* (Seismicity, Seismic Prediction, and Upper Mantle Properties in Relation to the Kamchatka Volcanism), Novosibirsk: Nauka, 1974, pp. 141–151.

Yanovskii, B.M., *Zemnoi magnetizm. Morfologiya i teoriya magnitnogo polya Zemli i ego variatsii* (Terrestrial Magnetism: The Morphology of the Earth's Magnetic Field and Its Variations), Leningrad: LGU, 1964.